PHYSICAL REVIEW B VOLUME 37, NUMBER 12 15 APRIL 1988-II

Nonlocal corrections to Fresnel optics: Model calculations from first principles for flat jellium

K. Kempa and W. L. Schaich
Physics Department and Materials Research Institute, Indiana University, Bloomington, Indiana 47405

(Received 20 July 1987)

New calculations of the Feibelman d parameters below the bulk-plasma frequency are presented for first-principles models of a jellium metal surface. We employ for the surface potential-energy barrier that confines the electrons the results found earlier by Lang and Kohn using a local-density-functional approach. The dynamic response is calculated both within the random-phase approximation and within the time-dependent local-density-functional approximation. There is little qualitative difference between the two when the density parameter $r_s=2$. Along with the d parameters, we exhibit the distribution of screening charge and total normal electric field. Various structures that appear in the frequency dependence of the response are identified and discussed.

I. INTRODUCTION

This paper continues our series of studies$^{1-4}$ of nonlocal corrections to Fresnel optics at metal surfaces based on calculations of induced screening charge. There has been considerable recent interest in this problem and several reviews$^{5-9}$ are available that discuss the wide range of application of the results. The sophistication of the model calculations has been steadily increasing and here we shall describe results for one of the best available descriptions of electronic structure at a flat, jellium surface. The response calculation can now be done in a manner consistent with the description of the ground state; i.e., both include exchange and correlation effects within a local-density-functional approximation (LDA). This improvement over the pioneering calculations of Feibelman,[10] which were done in the random-phase approximation (RPA), is of quantitative but not qualitative importance. Significant structures that appear as a function of frequency are essentially the same in both the LDA and RPA calculations.

In Sec. II we describe the modifications in our computational procedure that allow us to calculate the dynamic screening at any frequency below the bulk plasma frequency ω_p. Then in Sec. III we present results for a jellium surface with density parameter $r_s=2$. Examples of both the screening charge and field profiles in response to a time-dependent but (nearly) spatially constant perturbation are shown as well as the Feibelman d parameters. Based on our earlier calculations, one can give simple physical interpretations of the various structures that appear in the d's.

II. CALCULATIONAL METHODS

Our basic computational scheme remains the same as described in detail before.[2] However, to calculate efficiently with the inclusion of exchange and correlation effects we have changed the quantities directly found from the solution of the mean-field-integral equation. We briefly summarize these formal modifications first, following the notation and development of Ref. 2.

Start by writing the mean-field-integral equation for the induced electron density in real space, $\delta\rho(x)$, as

$$\delta\rho(x)=\int dx'\,\chi_0(x,x')\left[V_e(x')+\int dx''\,V_C(x',x'')\delta\rho(x'')+\delta\mu_{\mathrm{xc}}(x')\right]. \tag{1}$$

Here V_e is the (weak and slowly varying) external potential energy, the integral with V_C is the change in the Coulomb potential energy, $\delta\mu_{\mathrm{xc}}$ is the change in the effective single-particle potential energy due to exchange and correlation, and χ_0 is the independent particle susceptibility. We show explicitly only the dependence on the spatial coordinate normal to the surface, x; all the above quantities are at frequency ω and wave vector parallel to the surface $\mathbf{Q}$, the latter to be eventually set to zero. Like the Coulomb term, $\delta\mu_{\mathrm{xc}}$ is linear in the disturbance and within LDA is written as

$$\delta\mu_{\mathrm{xc}}(x)=V_{\mathrm{xc}}(x)\delta\rho(x) \tag{2}$$

with

$$V_{\mathrm{xc}}(x)=\left.\frac{d^2[n\varepsilon_{\mathrm{xc}}(n)]}{dn^2}\right|_{n=n_0(x)}, \tag{3}$$

where $\varepsilon_{\mathrm{xc}}$ is the exchange-correlation energy per electron in a uniform electron gas of density n and $n_0(x)$ is the equilibrium density of electrons at x in our surface problem.

We solve (1) by working with Fourier cosine transforms.[2] In this basis (1) becomes

$$\delta\rho(q)=\int dq'\,\chi_0(q,q')\left[V_e(q')+\delta\mu_{\mathrm{xc}}(q')+v(q')\delta\rho(q')-\gamma v(q')\int dq''\,v(q'')\delta\rho(q'')\right], \tag{4}$$

where we have used the separability of the off-diagonal part of $V_C(q,q')$. The factor γ is $[(Q/\pi)/4\pi e^2]$, where e is the electronic charge, and

$$v(q)=\frac{4\pi e^2}{Q^2+q^2} . \tag{5}$$

If we write $V_e(q)$ as $\gamma_e v(q)$, where γ_e is constant, and define

$$\lambda=\frac{\gamma}{\gamma_e}\int dq\, v(q)\delta\rho(q) \tag{6}$$

and

$$K(q,q')=\chi_0(q,q')v(q') , \tag{7}$$

then (4) may be expressed as

$$\delta\rho(q)=\int dq'\,K(q,q')[\gamma_e(1-\lambda)+\delta\mu_{\text{xc}}(q')/v(q')+\delta\rho(q')] . \tag{8}$$

Up to this point our analysis has followed that used earlier.[2] Now we depart slightly from it to write

$$\delta\mu_{\text{xc}}(q)=\gamma_e(1-\lambda)V_{\text{xc}}^{B}\,g(q) , \tag{9}$$

where $V_{\text{xc}}^{B}=V_{\text{xc}}(x\rightarrow\infty)$ is the bulk value of V_{xc}. Combining (2) and (9) yields

$$\delta\rho(q)=\gamma_e(1-\lambda)\alpha(q) , \tag{10}$$

with

$$\alpha(q)=\int dq'\Gamma(q,q')g(q') , \tag{11}$$

where

$$\Gamma(x,x')=\delta(x-x')V_{\text{xc}}^{B}/V_{\text{xc}}(x) . \tag{12}$$

Substituting (9)–(12) into (8) yields an integral equation for g,

$$\int dq'\left[\left[\Gamma(q,q')-K(q,q')\frac{V_{\text{xc}}^{B}}{v(q')}\right]g(q')-K(q,q')\int dq''\,\Gamma(q',q'')g(q'')\right]=\int dq'\,K(q,q') . \tag{13}$$

The computational task of solving (13) is clarified if we note the diagonal singularities in the Γ and K matrices

$$\Gamma(q,q')=\delta(q-q')+\overline{\Gamma}(q,q') , \tag{14}$$

$$K(q,q')=\chi_{0,B}(q)v(q)\delta(q-q')+\overline{K}(q,q') . \tag{15}$$

Here $\chi_{0,B}(q)$ is the bulk susceptibility,[2] related to the RPA dielectric function $\epsilon_B(q)$ by

$$\epsilon_B(q)=1-\chi_{0,B}(q)v(q) . \tag{16}$$

Incorporating (14)–(16), (13) becomes

$$\left[\epsilon_B(q)+[\epsilon_B(q)-1]\frac{V_{\text{xc}}^{B}}{v(q)}\right]g(q)-\int dq'\left[\overline{K}(q,q')\left[1+\frac{V_{\text{xc}}^{B}}{v(q')}\right]-\epsilon_B(q)\overline{\Gamma}(q,q')\right]g(q')$$
$$-\int dq'\int dq''\,\overline{K}(q,q')\overline{\Gamma}(q',q'')g(q'')=1-\epsilon_B(q)+\int dq'\,\overline{K}(q,q') , \tag{17}$$

which is the basic integral equation we solve. To make it reduce to the one solved for the RPA,[2] one sets $V_{\text{xc}}^{B}=0=\overline{\Gamma}$, so $g(q)=\alpha(q)$. Then writing $\alpha(q)=\nu(q)-1$, the equation for $\nu(q)$ is

$$\epsilon_B(q)\nu(q)-\int dq'\,\overline{K}(q,q')\nu(q')=1 , \tag{18}$$

which was treated in Ref. 2.

Our numerical method of solving either (17) or (18) consists of approximating the integral equation by a matrix equation of finite dimension. The complicated matrix is $\overline{K}(q,q')$, whose δ function and principal value singularities must be analytically isolated.[2] In fact we build this matrix in one long program and then store it. Two further short programs construct $\overline{\Gamma}$ and carry through the matrix algebra of (17) or (18).

Our new formal analysis has been designed to minimize the numerical problems with the second matrix, $\overline{\Gamma}(q,q')$ in (17). By rewriting (8) as an equation for $g(q)$ (i.e., $\delta\mu_{\text{xc}}$) rather than for $\alpha(q)$ (i.e., $\delta\rho$), we need to transform $1/V_{\text{xc}}(x)$ rather than $V_{\text{xc}}(x)$. This is convenient because $V_{\text{xc}}(x)$ if determined from (3) diverges roughly as $n_0^{-2/3}(x)$ when x moves into vacuum. Hence the matrix Γ shows less sensitivity to the origin of the cosine transforms than does its inverse. The physical picture is that both $\delta\mu_{\text{xc}}(x)/V_{\text{xc}}^{B}$ and $\delta\rho(x)$ eventually tend to zero outside the metal, but are related by (2). Given that we can solve the relevant integral equations only to a fixed accuracy, it is numerically preferable to solve for the larger quantity, $\delta\mu_{\text{xc}}(x)/V_{\text{xc}}^{B}$, from an integral equation and then find the smaller quantity $\delta\rho$ from (2), rather than the other way around.

Since we have already described the formal structure of $K(q,q')$[2], we comment here only on the new features that arise in the present calculations. We now use about half as many mesh points as before, both to save time and because we have a better sense of where they are needed. The spatial variation of the single-particle orbitals near the surface is found from a Noumerov integration routine.[11] These wave functions are computed, stored, and then combined to form $K(q,q')$. The slowest step comes from the double surface integral, Eq. (73) in Ref. 2. Unlike the procedure of Gies, Gerhardts, and Maniv[12] we must redo everything when the frequency is changed. In the k integrations over occupied states we have found it helpful to do analytically, where possible, cases that involve explicit factors of $(\hbar^2k^2/2m - \hbar\omega)^{1/2}$, as in the N functions of Eq. (67) in Ref. 2. This improvement is especially important for extending the calculations below $0.3\omega_p$, no matter what the surface-barrier shape. The matrix elements of $\bar{K}(q,q')$ for q or q' greater than several times the Fermi wave vector k_F are of negligible consequence. To avoid the considerable effort of their accurate calculation, we simply set

$$\bar{K}(q,q')=0 \text{ for } q,q'>q_c\ , \tag{19}$$

where the cutoff wave vector q_c lies between three and four times k_F. We also have numerical difficulties with the matrix elements for arbitrarily small q', due to the Coulomb factor $v(q')$ in (7). However, since the results for $g(q)$ seem to be smooth functions of q as $q \rightarrow 0$, we can extrapolate if necessary to the smallest values of q from larger, more numerically tractable values. The above remarks apply to any surface-barrier model for which the wave functions are found by numerical integration. By solving a single-step barrier model with either numerical or analytical wave functions we were able to check the validity of the various cutoffs and extrapolations.

We end this section by pointing out how the ingredients differ between a calculation with a Lang-Kohn barrier[13] and one with a step barrier. Since the Lang-Kohn barrier is more diffuse, we need to use in that case a larger value of the parameter a, which is the distance between where the occupied wave functions have become negligible in vacuum and where the effective potential energy in the metal has saturated as its bulk value. This larger value of a leads to a more rapid modulation of all wave-vector dependences and requires a finer mesh when we convert integrals to sums. The more diffuse barrier also enhances the phase shift $\phi(k)$ that an electron with normal wave vector k in bulk undergoes when scattering from it, as shown in Fig. 1. Note especially the large and rapid variation of ϕ when the electron's normal kinetic energy, $\hbar^2k^2/2m$, is close to the total barrier height. We must be careful when choosing our integration meshes to have extra points in this energy region if it is accessible by the final-state electrons. We remark that a better treatment of the surface barrier, in which its deviation from its vacuum limit asymptotically varies as an image attraction proportional to $|x|^{-1}$ rather than going exponentially in x as in LDA, would exacerbate the problem. The near singular structure in ϕ near the photoemission threshold extends through the whole calculation to influence structure in $g(q)$, $\alpha(q)$, $\delta\rho(x)$, and $d_\perp(\omega)$.

III. RESULTS

The quantities we present are a normalized $\delta\rho(x)$, $\eta(x)$, and $d_\perp$, where

$$k_F\int_0^\infty dx\,\delta\rho(x)=1\ , \tag{20}$$

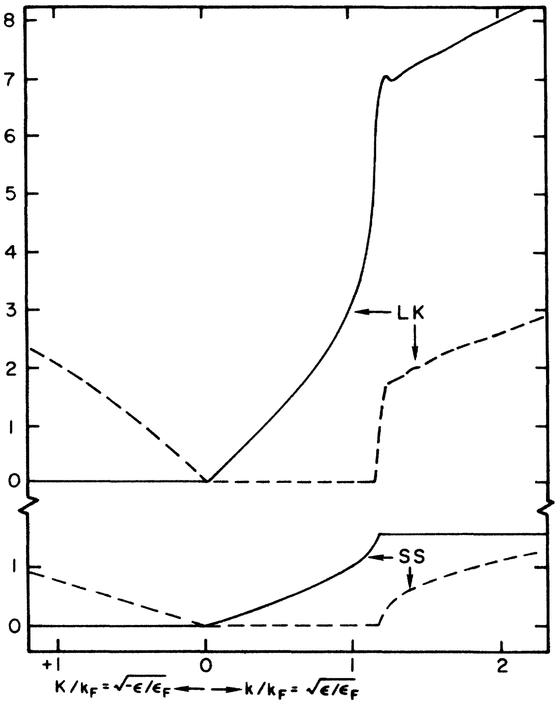

FIG. 1. Phase shift ϕ vs normal wave vector k or K for two different surface barriers. The wave function for motion normal to the surface plane is assumed to vary as $\sin[(\varepsilon/\varepsilon_F)^{1/2}k_Fx+\phi]$ for $x>0$ where the potential energy has saturated at its bulk value which we set to zero. The solid (dashed) curves give the real (imaginary) part of ϕ. The wave vectors, scaled by the Fermi wave vector k_F, are found from the normal kinetic-energy ε scaled by the Fermi energy ε_F. The LK curves are for the Lang-Kohn barrier at $r_s=2$ (Ref. 13), while the SS curves are for a single-step barrier model of Al (Refs. 2 and 3) with $r_s=2.07$. The work functions for the two barriers differ by $0.05\varepsilon_F$. The small differences in the bulk density parameters and in the work functions are not the cause of the large differences in ϕ.

$$\eta(x)=k_F\int_0^x dx'\,\delta\rho(x')\ , \tag{21}$$

and

$$d_\perp=\int_0^\infty dx\,x\delta\rho(x)\Big/\int_0^\infty dx\,\delta\rho(x)\ . \tag{22}$$

Here k_F is the bulk Fermi wave vector and the origin for x in these equations has been placed where the cosine transforms begin, which is far enough into vacuum for the occupied wave functions to have decayed to negligible values. Our program calculates the above quantities from the function $\nu(q)$ using

$$\delta\rho(x)=\frac{2}{\pi}\int_0^\infty \frac{dq}{k_F}\cos(qx)\left[\frac{\nu(q)-1}{1/\epsilon_B-1}\right]\ , \tag{23}$$

$$\eta(x)=\frac{2}{\pi}\int_0^\infty \frac{dq}{q}\sin(qx)\left[\frac{\nu(q)-1}{1/\epsilon_B-1}\right]\ , \tag{24}$$

and

$$d_\perp = \frac{2}{\pi}\int_0^\infty \frac{dq}{q^2}\left[\frac{v(q)-1/\epsilon_B}{1-1/\epsilon_B}\right], \tag{25}$$

where $\epsilon_B = 1-\omega_p^2/\omega^2$ is the long-wavelength limit of the bulk dielectric function. Equations (22) and (25) are valid only if $\omega < \omega_p$.

As discussed before,[3] within a local optics (Fresnel) model of a single interface $\delta\rho$ is a δ function and η is a unit step function. They represent, respectively, the sheet of screening charge produced by the metal and the consequent jump in the normal component of the total electric field. Our interest lies with how these singular behaviors across a (fictitious) matching plane are smeared out in more realistic models.

We begin by showing RPA results in Fig. 2 for the Feibelman d parameters. We have plotted the origin-independent quantity $d_\perp - d_\parallel$, where the constant, positive background charge density (the jellium) sits in $x \geq d_\parallel$. For the models treated here the imaginary part of $d_\perp - d_\parallel$, $\mathrm{Im}(d_\perp - d_\parallel)$, must be negative for $\omega < \omega_p$ since it is directly related to the absorption of energy.[5] However, the real part of $d_\perp - d_\parallel$, $\mathrm{Re}(d_\perp - d_\parallel)$, may have either sign and indeed for the Lang-Kohn barrier passes through zero at about $\omega/\omega_p \simeq 0.8$.

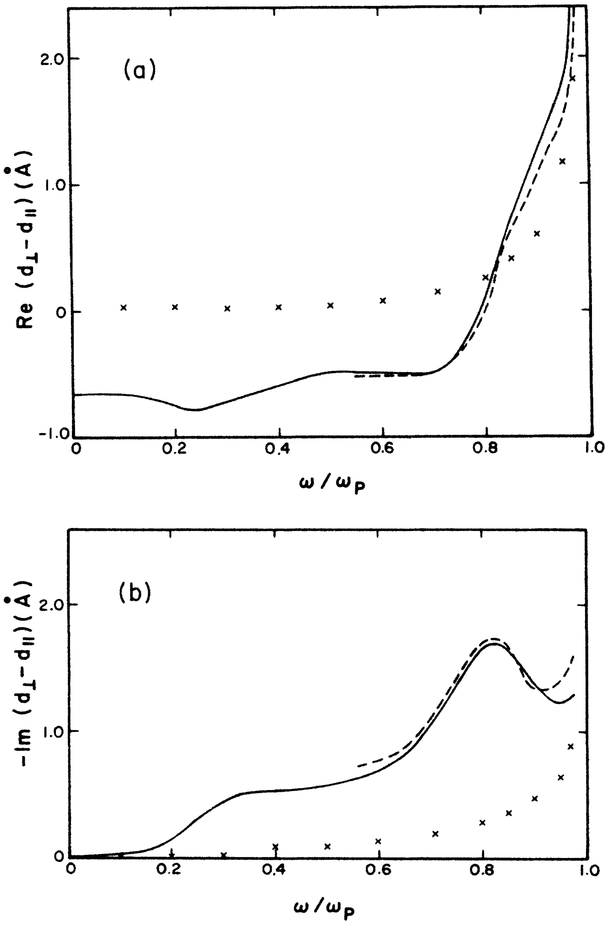

FIG. 2. Feibelman d parameters vs frequency by RPA calculations. The solid curve is from the present calculation for a Lang-Kohn barrier model at $r_s = 2$, while the dashed curve represents the results of Feibelman for the same model. The crosses are from a calculation for a single-step barrier model of Al, whose parameters are given in the text.

For comparison with the new calculations, we also plot Feibelman's results for the same jellium model and results for a simpler, single-step barrier model. One sees that our values agree quite well with Feibelman's except for ω close to ω_p. By using different integration meshes and extrapolations it appears that our answers for $\omega > 0.9\omega_p$ are uncertain by at least ±0.1 Å, which can almost account for the differences with Feibelman, especially since the inaccuracy in his results is not stated. At lower ω our absolute accuracy improves and we have no trouble going below $\omega_p/2$, where Feibelman had to stop his calculations due to numerical difficulties. However, our relative inaccuracy in $\mathrm{Im}(d_\perp - d_\parallel)$ for $\omega \leq 0.1\omega_p$ precludes a useful determination of its limiting slope.

The other results shown in Fig. 2 are for a single-step barrier model of Al. In this model, $r_s = 2.07$ and the surface-barrier height scaled by the Fermi energy is 1.356, rather than 1.304, as in the $r_2 = 2$ Lang-Kohn model. These minor numerical changes are not responsible for the large differences in the calculated d parameters. Rather it is change in the shape of the potential-energy barrier at the surface of the metal that leads to the differences. We will discuss specific features below after we describe the modifications due to the inclusion of exchange and correlation in the dynamic response.

These changes are shown in Fig. 3 and are relatively minor. On a qualitative level, at least for $r_s = 2$, there is no significant difference between the RPA and the LDA results. This is also apparent in Fig. 4, which shows the induced screening charge profile at $\omega/\omega_p = 0.55$ based on the solution of either (17) or (18). There are quantitative differences, such as the enhancement in Fig. 3 of the limiting slope of $\mathrm{Im}(d_\perp - d_\parallel)$ in LDA; but the large-scale structures, to which we now turn, are essentially the same.

At the extremes of our frequency range there are common patterns of behavior which are seen in all model calculations.[3] As $\omega \to 0$, $\mathrm{Im}(d_\perp - d_\parallel)$ goes linearly to zero while $\mathrm{Re}(d_\perp - d_\parallel)$ saturates at the static image plane position. The actual values of the corresponding limiting slope and intercept are sensitive functions of the surface-barrier model. At the other extreme as $\omega \to \omega_p$, both the real and imaginary parts of $d_\perp$ diverge due to the incipient excitation of the bulk plasmon. The divergence is weaker than $(\omega-\omega_p)^{-1}$ but we cannot determine whether it is proportional to the analytic estimate $(\omega-\omega_p)^{-1/2}$ of simpler models.[3]

Our difficulty in extracting quantitative measures of the limiting behaviors is only partly due to our numerical problems near $\omega = 0$ or $\omega = \omega_p$. The situation is also complicated by the small frequency range over which the limiting behavior appears to hold. There are two specific structures in the curves whose form is clearly different from the limiting behavior, but whose locations for $r_s = 2$ are close to the extremes. We associate the low-frequency structure with the threshold for photoemission, which occurs at $\omega/\omega_p = 0.23$ for the $r_s = 2$, Lang-Kohn barrier. As ω rises through this level there is a steplike increase in $\mathrm{Im}(d_\perp - d_\parallel)$ and a corresponding dip in $\mathrm{Re}(d_\perp - d_\parallel)$. At a qualitative level the effect is also present in the single-step barrier results of Fig. 2, but the size of the absorption is nearly an order of magnitude less than for the Lang-Kohn barrier. We remark that the present single-step results differ below the photoemission threshold from those presented in Ref. 3. The latter shows a minimum in $-\mathrm{Im} d_\perp$ versus ω which arose from numerical problems that have now been corrected. However, we still trust the structure shown in calculations on another single-step barrier model[1] and we did confirm that the minimum in $-\mathrm{Im} d_\perp$ seen there occurs when one sweeps either frequency or barrier height through a threshold for photoemission.

There are significant changes in the profile of the screening charge density as ω moves through the photoemission threshold. Figure 5 contrasts the behavior on either side. From Fig. 3 one expects to see an enhancement in the imaginary part of $\delta\rho$. This does occur, but the real part of $\delta\rho$ also changes noticeably, shifting towards the jellium and modifying its period of Friedel oscillations. As discussed in Sec. II, the latter is a consequence of the sharp structure of the phase shift (shown in Fig. 1) influencing the excited state Green's function above threshold. We note in passing that the alternate calculations of Gies, Gerhardts, and Maniv[12] do not properly describe the photoemission structure since their surface potential-energy barrier is for numerical convenience raised to infinity just outside the jellium, thereby suppressing the possibility of photoemission.

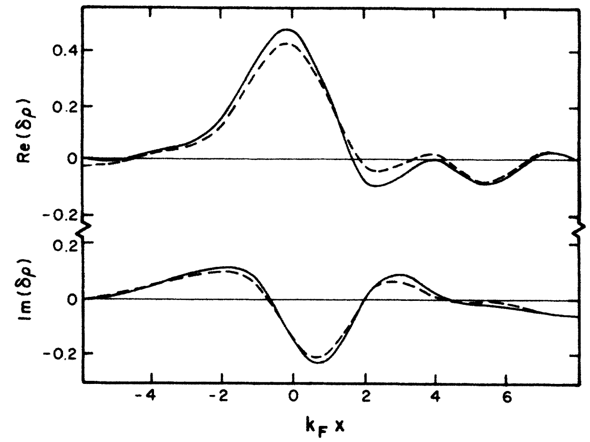

FIG. 4. Real and imaginary parts of the induced charge density vs distance along the surface normal, calculated within either LDA (solid curves) or RPA (dashed curves). The perturbation is at the frequency $0.55\omega_p$. The origin has been placed so the jellium sits in $x > 0$, and distances are scaled by the bulk Fermi wave vector k_F.

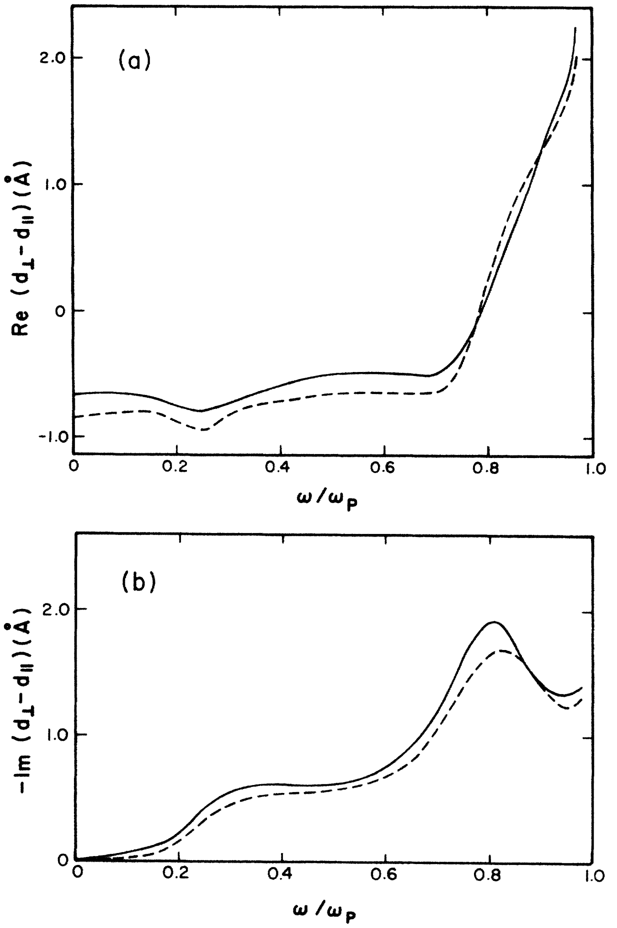

FIG. 3. Feibelman d parameters vs frequency by either LDA calculation [(a) dashed curve, (b) solid curve] or RPA calculations [(a) solid curve, (b) dashed curve]. Both calculations use the same Lang-Kohn, $r_s = 2$ barrier.

The other clear structure in Figs. 2 and 3 is centered about $\omega = 0.8\omega_p$. We interpret it as due to the existence of an extra surface collective mode (ESCM) and stress that for $r_s \simeq 2$ it is absent from the single-step barrier model (as well as from the infinite barrier model[3,14]). Within hydrodynamic models, such additional modes can be produced by making the equilibrium density profile

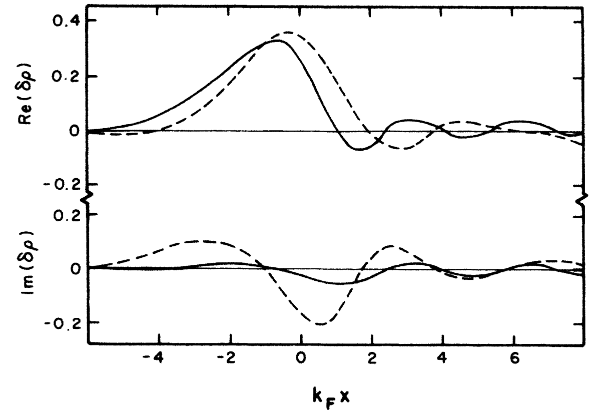

FIG. 5. Real and imaginary parts of the LDA induced charge density vs distance along the surface normal. The perturbing frequency is either just below ($\omega/\omega_p = 0.1$, solid curves) or just above ($\omega/\omega_p = 0.4$, dashed curves) the photoemission threshold. The abscissa is the same as in Fig. 4.

sufficiently diffuse. These calculations lead to the picture of the ESCM as plasma waves trapped within a local plateau of the equilibrium profile.[15] Although it requires some extrapolation, we feel that this physical picture is helpful[16,17] in understanding the structure found here for the Lang-Kohn barrier. We acknowledge that there is no obvious density plateau in the equilibrium Lang-Kohn profile and that particle-hole excitations are essentially ignored by models that focus on standing plasma waves. Still, when we compare the qualitative behavior of the screening charge and total normal field as ω passes through the "mode," there is a considerable similarity to results found in a model that definitely contains a standing plasma-wave resonance.[4] To this end we plot in Fig. 6 both $\delta\rho$ and η for ω near $0.8\omega_p$. This figure should be compared to Fig. 3 in Ref. 2, which was calculated for a (double-step potential barrier) model of one monolayer of Na on an Al substrate. The resonance behavior is seen most clearly in the imaginary parts of $\delta\rho$ and η. Note the dipolar shape of $\mathrm{Im}\delta\rho$ and the large surface peak in $\mathrm{Im}\eta$. Experimental corroboration of this structure in this dissipative response has been developed from photoemission studies.[18] The real parts of the response properties also have a characteristic behavior since $\mathrm{Re}(d_\perp - d_\parallel)$ moves rapidly from outside to inside the jellium as ω sweeps through the mode. This is evident in Fig. 6 as for instance by the shift in the location of $\mathrm{Re}(\eta)=0.5$. Note too the development of a negative dip in both $\mathrm{Re}(\delta\rho)$ and $\mathrm{Re}(\eta)$ outside the jellium. These features are weaker in the present Lang-Kohn, clean-surface model than they are in the double-step, overlayer model,[4] yet we feel that they are the remnants of the same physical phenomenon.

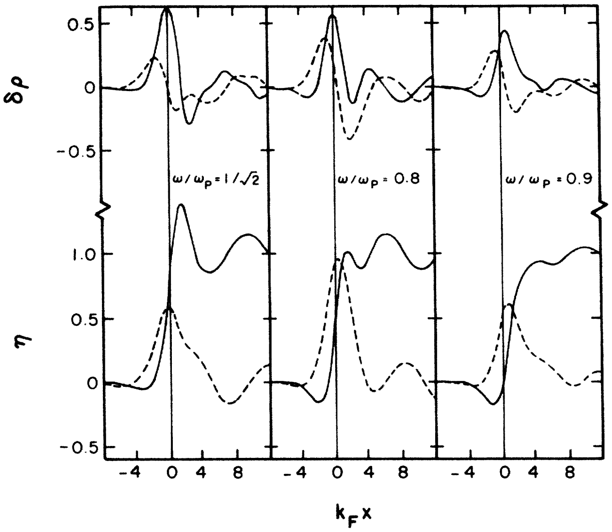

FIG. 6. Real and imaginary parts of the induced charge density and total normal field calculated within LDA vs distance along the surface normal. The various perturbation frequencies are noted and the real (imaginary) parts are plotted as solid (dashed) lines. The abscissa has the same units and origin as in Fig. 4.

ACKNOWLEDGMENTS

We thank Dr. N. D. Lang for sending us the numerical output describing his surface barriers and Dr. P. J. Feibelman for sending us his numerical results for the d parameters. The major calculations were performed on the Cray 48 X-MP run by the National Center for Supercomputing Applications at the University of Illinois. Our time allowance there as well as other partial support were provided by the National Science Foundation through Grant No. DMR 85-12709.

---

[1] K. Kempa and W. L. Schaich, Phys. Rev. B **32**, 8375 (1985).

[2] K. Kempa and W. L. Schaich, Phys. Rev. B **34**, 547 (1986).

[3] W. L. Schaich and K. Kempa, Phys. Scr. **35**, 204 (1987).

[4] K. Kempa and W. L. Schaich, Solid State Commun. **61**, 357 (1987).

[5] P. J. Feibelman, Prog. Surf. Sci. **12**, 287 (1982).

[6] F. Forstmann and R. R. Gerhardts, in *Festkörperprobleme*, edited by J. Treusch (Vieweg, Braunschweig, 1982), Vol. 21, p. 291.

[7] P. Apell, A. Lyungbert, and S. Lundqvist, Phys. Scr. **30**, 367 (1984).

[8] F. Forstmann and R. Gerhardts, *Metal Optics Near the Plasma Frequency* (Springer, Berlin, 1986).

[9] A. Liebsch, Phys. Scr. **35**, 354 (1987).

[10] P. J. Feibelman, Phys. Rev. B **12**, 1319 (1975).

[11] J. M. Blatt, J. Comput. Phys. **1**, 382 (1967).

[12] P. Gies, R. R. Gerhardts, and T. Maniv, Phys. Rev. B **35**, 458 (1987).

[13] N. D. Lang and W. Kohn, Phys. Rev. B **1**, 4555 (1970).

[14] R. R. Gerhardts and K. Kempa, Phys. Rev. B **30**, 5704 (1984).

[15] C. Schwartz and W. L. Schaich, Phys. Rev. B **26**, 7008 (1982).

[16] C. Schwartz and W. L. Schaich, Phys. Rev. B **30**, 1059 (1984).

[17] K. Kempa and R. R. Gerhardts, Solid State Commun. **53**, 579 (1985).

[18] H. J. Levinson, E. W. Plummer, and P. J. Feibelman, Phys. Rev. Lett. **43**, 952 (1979).